D13

N79-24014

SPACECRAFT CHARGING RESULTS FOR THE DSCS-III SATELLITE

Michael J. Massaro and Dale Ling
General Electric Space Division

ABSTRACT

Spacecraft charging results are presented for the DSCS-III satellite for a severe geomagnetic substorm. Spacecraft charging results were obtained by the use of the Electrostatic Charging Analysis Program (ESCAP). The ESCAP computer code which can determine both the transient or steady-state differential charging potentials is an engineering design tool that utilizes a circuit theory approach to spacecraft charging. Using the ESCAP code, the steady-state (static) differential potentials of the outer spacecraft surfaces and metallic structure were obtained for the DSCS-III satellite when under the influence of a severe geomagnetic substorm during the local midnight-to-dawn quadrant of its geosynchronous orbital path. The results obtained indicate that, in the steady-state, most of the DSCS-III outer surface materials will not achieve differential potentials large enough to produce an electrostatic discharge (ESD). Recent changes to the ESCAP code to improve execution time are discussed as well as model improvements for future development.

INTRODUCTION

The main purpose of this paper is to present the results of a spacecraft charging analysis of the DSCS-III satellite. (DSCS-III is the third generation satellite of the Defense Satellite Communication System.) In addition, a discussion of an approach to determine the probabilistic rate of electrostatic discharge (ESD) of dielectric materials is presented. Spacecraft charging refers to that phenomenon whereby the outer materials of spacecraft attain surface charges produced by the bombardment of energetic charged particles. During a geomagnetic substorm the outer dielectric surfaces can achieve differential potentials at which electrostatic discharge (ESD) can occur. ESD can cause degradation of the thermal properties of materials, state changes of operational circuitry, and RF interference to receivers. Thus, it is important to determine if any of the outer dielectric materials, will be a source of ESD.

Spacecraft charging results were obtained by using the Electrostatic Charging Analysis Program (ESCAP) which was developed by the General Electric Space Division under an internally funded research program. The ESCAP code can determine both the transient and steady-state differential potentials; however, at present, only the steady-state solutions can be obtained with a

reasonable amount of computer time (20-30 minutes of main-frame computer time for 1 to 3 minutes of transient results versus 5-10 seconds of main-frame time for a complete steady-state solution). The ESCAP code utilizes a circuit theory approach to spacecraft charging. The spacecraft-to-environment interaction is determined by representing the charged particle environment as equivalent current source functions and by representing the spacecraft by its electrically equivalent circuit with respect to the plasma charging phenomenon. The charging model includes a sun/earth/spacecraft orbit model that simulates the sun illumination conditions of the spacecraft outer surfaces throughout the geosynchronous orbit.

Recent changes to decrease the computer time needed to execute a steady-state solution are discussed as well as improvements in the plasma current source representation. In addition, the variation of S/C charging differential potentials as a function of the secondary electron emission coefficient is presented.

The paper is organized as follows. First, a brief description of ESCAP is given. The S/C charging results for the DSCS-III satellite are presented along with a description of its material and geometric configuration and the pertinent plasma and emission parameters used in the analysis. Next, ESD probabilities of occurrence are derived and lastly, the ESCAP code improvements are discussed.

SPACECRAFT CHARGING MODEL

The spacecraft charging model can best be described in terms of the flow chart shown in figure 1. The ESCAP code consists of four separate models: a plasma model, an electrical model, a S/C geometrical model; and a solar/earth/orbital model. The plasma model represents the charging and discharging mechanism of the ambient plasma with respect to the spacecraft by equivalent current sources. The current sources, which are dependent on the particle energy distribution functions, constitute the forcing functions of the charging model equations. At present, the plasma generated current sources are assumed to have a single, omnidirectional Maxwellian energy distribution with time-independent parameters for the duration of the subsystem. However, the model can be easily modified to consider a "two- Maxwellian" energy distribution plasma representation as well as field-aligned fluxes. The approach to accomplish this is discussed in a later section.

The electrical model defines the lumped element equivalent circuit representation of the spacecraft surfaces with respect to the electrostatic charging phenomenon. The plasma model and electrical model are combined to form the non-linear spacecraft charging equations. The spacecraft geometrical model defines the spacecraft outer surfaces in terms of approximate planar surfaces and curved surface projections and defines the vertices of all planar and curved surfaces in terms of a spacecraft reference coordinate system. The solar/earth/orbital model determines the location of the spacecraft with respect to the sun and the earth. The geometrical model and the

solar/earth/orbital model are combined to determine the variation of the sun-illumination conditions of the outer surfaces with respect to orbital position.

To complete the modeling, the surface material properties and configuration are defined. The surface material properties that are most important in a spacecraft charging analysis are the relative dielectric constant; the variation of the surface resistivity with respect to electrical stress level; and the variation of the bulk resistivity with respect to electrical stress level. The material configuration definition describes the location of the various thermal blanket and surface coating materials.

A more detailed description of the program is given in reference 1.

MATERIAL AND GEOMETRIC CONFIGURATION

DSCS-III is a three-axis stabilized spacecraft operating in a geosynchronous orbit. The spacecraft has two nineteen beam transmit multiple beam antennas, a sixty-one beam receive multiple beam antenna, two earth coverage receive antennas, two earth coverage transmit antennas, a gimballed dish transmit antenna (GDA), and a receive antenna and a transmit antenna for the Single Channel Transponder (SCT). The main body of the spacecraft is almost cube shaped with the approximate dimensions shown in figure 2. Also shown in figure 2 is the outer thermal blanket material and coating configuration. A summary of the thermal blanket material properties and locations is given in table 1. To prevent the fiberglass structural parts of the SCT antennas from becoming a source of ESD, the fiberglass surfaces were coated with conductive Indium Tin Oxide (ITO). The thickness of the conductive coating was chosen to promote a gradual depletion of the surface charge to the structure with minimal effect on the RF performance of the SCT antennas. From similar coating processes it has been found that a minimum total surface resistance of 500 K Ω can be expected for ITO. The bulk resistivity values listed in table 1 are the values measured at a low voltage level; however, the actual bulk resistivity characteristics, i.e., bulk resistivity as a function of the potential across the material, were employed in the analysis. A summary of the areas of the outer thermal blanket materials and coatings is given in table 2. The amount of exposed structural metal is also listed as well as those surfaces that are never exposed to direct radiation from the sun, i.e., the "permanently shadowed" areas.

PLASMA PARAMETERS AND SPACECRAFT CHARGING EQUATIONS

Recently there has been considerable effort to refine and expand the plasma substorm environmental data base, that is, the diurnal variation of the parameters that characterize the plasma substorm particle density and energy distributions. In particular, the Air Force Geophysical Laboratories (AFGL) has established a computer based plasma substorm parameter data file (ref. 2)

which contains parameters for a "one" Maxwellian or "two" Maxwellian approximation to the actual measured plasma distribution. AFGL supplied the Space Division with a representative range of plasma substorm parameter values. Part of the information supplied was a single Maxwellian distribution function approximation of the actual measured particle density and energy distributions. The single Maxwellian distribution approximation parameters were used in the ESCAP program. The range of plasma particle temperatures and current densitites supplied by AFGL and the range of secondary and photoemission parameters obtained from the literature are presented in table 3.

Also shown in table 3 are the parameter values selected for use in the ESCAP program. Three levels of substorm activity were established: mild, moderate, and severe. Since the electron particles have the greatest influence on spacecraft charging, the electron current density and energy values were used to classify the substorm. Spacecraft charging results were obtained for all three levels of substorms; however, only the results for the severe substorm will be presented herein.

The equivalent plasma and photoemission generated current sources were derived in reference 1 and are based on a "single Maxwellian" approximation to the actual plasma particle energy distribution functions. Incident protons and electrons as well as secondary electrons and photoelectrons were considered in the plasma model. For a large dielectric surface, the current forcing function will have the general form (see ref. 1)

$$I_D(V) = \left[\left(J_{po}e^{-V/T_p}\right)\left(1 + f_{pd}e^{-V/T_s}\right) + \left(J_{pho}\right)_d (\cos\alpha)e^{-V/T_{ph}} + \left(J_{eo}e^{V/T_e}\right)\left(f_{ed}e^{-V/T_s} - 1\right)\right] \cdot A \qquad (1)$$

where I_D is the total positive current into a large dielectric surface, A is the area of the surface, J_{eo} is the average ambient electron current density incident to a neutral surface, J_{po} is the average ambient proton current density incident to a neutral surface, $(J_{pho})_d$ is the average photoelectron current density emitted from an illuminated neutral dielectric surface, V is the absolute potential of the dielectric surface, T_e is the equivalent temperature, expressed in volts, of the Maxwell-Boltzmann (M-B) distribution approximating the plasma electron energy distribution, T_p is the equivalent temperature of the M-B distribution approximating the plasma proton energy distribution and is expressed in volts, T_s is the equivalent temperature of the M-B distribution representing the energy distribution of the secondary emission electrons and is expressed in volts, T_{ph} is the equivalent temperature of the M-B distribution representing the energy distribution of the photoelectrons expressed in volts, f_{ed} is the secondary electron emission coefficient for electrons incident to a dielectric surface, f_{pd} is the secondary electron emission

coefficient for protons incident to a dielectric surface, and α is the sun aspect angle for the dielectric surface.

The above equation must satisfy the following condition

$$e^{sV/X} = \begin{cases} 1 \text{ if } s = +1 \text{ and } V > 0; \text{ otherwise leave unchanged} \\ \\ 1 \text{ if } s = -1 \text{ and } V \leq 0; \text{ otherwise leave unchanged} \end{cases}$$

The sun aspect angle, α, is the angle between the sun-line and the surface normal vector and

$$\cos \alpha = \begin{cases} \cos \alpha & \text{for } |\alpha| < \pi/2 \\ 0 & \text{for } |\alpha| \geq \pi/2 \quad \text{(self-shadowing conditions)} \end{cases} \tag{3}$$

The positive current flowing into the metallic structure is (see ref. 1)

$$I_M(V) = A_{MT}J_{po}(1 + V/T_p)e^{-V/T_p}\left(1 + f_{pm}e^{-V/T_s}\right) + A_{MT}J_{eo}e^{V/T_e}\left(f_{em}e^{-V/T_s} - 1\right)(1 + |V/T_e|) + \sum_{i=1}^{m} A_{Mi}(J_{pho})_m (\cos \alpha_i)e^{-V/T_{ph}} \tag{4}$$

where equations (2) and (3) hold for the above equation and A_{MT} is the total exposed metallic area, A_{Mi} is the exposed area of the i^{th} metallic surface, m is the total number of exposed metallic surfaces, α_i is the sun aspect angle for the i^{th} metallic surface, f_{pm} is the secondary electron emission coefficient for protons incident to a surface, metallic f_{em} is the secondary electron emission coefficient for electrons incident to a metallic surface, and the following holds for the small area correction terms

$$(1 + V/T_p) = \begin{cases} (1 + V/T_p) \text{ for } V \geq 0 \\ 1 \text{ for } V < 0 \end{cases} \quad (5)$$

$$(1 + |V/T_e|) = \begin{cases} (1 + |V/T_e|) \text{ for } V \leq 0 \\ 1 \text{ for } V > 0 \end{cases} \quad (6)$$

The lumped element, equivalent electrical circuit representation of the spacecraft outer surfaces with respect to the electrostatic charging phenomenon was derived in reference 1 and is shown in figure 3. The steady-state spacecraft charging equations for the simplified circuit of figure 3 are given by

$$\frac{V_1 - V_o}{R_1 (V_1 - V_o)} = I_1 (V_1) \quad (7)$$

$$\vdots \qquad \vdots$$

$$\frac{V_n - V_o}{R_n (V_n - V_o)} = I_n (V_n) \quad (8)$$

$$\sum_{i=0}^{n} I_i = 0$$

It has been assumed that there are n outer surfaces. The i^{th} surface has an absolute potential of V_i volts and each surface, or node, has a corresponding plasma and photoemission generated current source, I_i, having the general form of equation (1). The spacecraft structure has an absolute potential of V_o volts and I_o is the plasma and photoemission generated current source into the exposed metallic surfaces and is given by equation (4). Equations (7) and (8) in general, will be non-linear since the leakage resistances are non-linear functions of stress level $(V_i - V_o)$ and the plasma currents are non-linear functions of stress level also, i.e., voltage dependent current sources.

The number of equations, n, is a function of both the number of surfaces with different materials and with different sun illumination conditions, i.e., the number of surfaces with different orientations with respect to the spacecraft reference coordinate system. The solution of this set of n simultaneous nonlinear equations is discussed in a later section.

SPACECRAFT CHARGING RESULTS

Spacecraft charging results were obtained for the peak of the winter-solstice and fall-equinox orbital periods for a severe substorm. It was assumed that the plasma substorm had a duration of nine hours starting at 23:00 LT and ending at 8:00 LT. The extremes of spacecraft response are obtained during these two orbital periods. For example, during equinox the spacecraft will experience eclipse conditions (total-shadowing) and the spacecraft structure achieves its highest negative potential; whereas during winter-solstice the spacecraft structure achieves its lowest negative potential. The latter condition results from the fact that the South Panel has more exposed metal than the North Panel and that during winter-solstice the South Panel is illuminated by the sun. The OSR coverglass material exhibited the greatest steady-state potential difference, i.e., the potential difference between the outer surface and the spacecraft structure. The steady-state potential differences of the above material as well as the absolute potential of the spacecraft structure during a severe substorm are listed in tables 4 and 5, for fall-equinox and winter-solstice, respectively. It can be seeen from these tables that the spacecraft structure achieves a maximum negative absolute potential of -14 kV during eclipse and a minimum negative absolute potential of -170 V during winter-solstice. The OSR coverglass material achieves its greatest potential difference during winter-solstice. The steady-state absolute potentials of all of the spacecraft outer surfaces for a severe substorm are shown in figures 4 and 5 for fall-equinox and winter-solstice at 8:00 LT, respectively.

A summary of the maximum steady-state potential differences achieved by all of the outer surfaces during the fall-equinox and winter-solstice orbital periods is listed in table 6. It can be seen from table 6 that the OSR coverglass achieved the highest steady-state potential difference, 5200 volts. Because of the potential differences attained by the OSR coverglass, this material may be a possible source of ESD and the OSR coverglass material will be the only steady-state source of ESD during a severe substorm. Electron bombardment tests of this material have indicated that low-level, observable discharges will occur at potential differences on the order of 7 kV. In order to assess the effects of the ESD produced by the OSR coverglass on the performance of the DSCS-III system both the radiated ESD field levels and the rate of ESD had to be determined. Measured values of the magnitude of radiated ESD fields are presented in reference 3 and an estimate of the probabilistic occurrence rate of ESD is derived in the following section.

Finally, it should be mentioned that the above spacecraft charging analysis considered only the steady-state potential differences. It is possible for the solar array coverglass to produce ESD because of transient potential differences between the coverglass and the spacecraft metallic structure. However, these discharges, if any, will be produced only during severe substorms and only when the spacecraft enters and exits eclipse.

ESD PROBABILITIES OF OCCURRENCE

In order to determine the probabilities of occurrence of ESD from OSR coverglass, a sample of the material was subjected to electron bombardment tests to simulate a severe substorm environment. The OSR Glass was bombarded with electrons having an accelerating potential of 20KeV and a density of $1.5 na/cm^2$. This current density value is about twice the maximum electron current density of any plasma substorm that has been measured up to the present time. Discharges were observed at the rate of about one every twenty seconds. Since there are twenty separate sections of OSR glass on DSCS III (each section consisting of hundreds of cells of OSR glass) and since each section can discharge independently, a binomial probability density function was used to characterize the statistical occurrence of ESD from OSR coverglass. Thus, the probability of k discharges in Δt seconds is

$$P(k) = \binom{n}{k} p^k q^{n-k} \tag{9}$$

where P(k) is the probability of k discharges in Δt seconds, n is the number of sections of OSR glass, 20, p is the probability of a discharge occurring in Δt seconds and q is the probability of no discharge in Δt seconds. For the OSR cover glass there results

$$p = \frac{\Delta t}{T}$$

$$q = \overline{p} = (1-p) \tag{10}$$

where T is the periodicity of a discharge for one section of OSR glass and is equal to about 20 seconds for the simulated substorm. The probability of m-or-more discharges occurring in one second is the complement of the probability of (m-1)-or-less discharges occurring and from equation (7) is given by

$$\text{Pr(m-or-more discharges)} = 1-\text{Pr((m-1)-or-less discharges)} = 1-\sum_{k=0}^{m-1} P(k) \tag{11}$$

Using equation (11), the ESD probabilities of occurrence were computed for one-or-more up to ten-or-more discharges occurring randomly in one second and the results are presented in table 7. It can be seen from table 7 that the probability of ten-or-more discharges occurring per second is extremely

remote; whereas, there is a high probability that at least one discharge will occur each second.

In the above formulation it has been assumed that each section of OSR glass, independent of the number of cells per section, will have the same discharge rate as the nine cell sample that was tested. This assumption is valid if there is a tendency for most of the cells to be affected by the discharge process.

Variation of Differential Potential with Secondary Emission

In the simplified spacecraft charging approach presented herein, the secondary electron emission coefficients were assumed to be a constant value, .5 for metals and .75 for dielectrics. To determine the sensitivity of the steady-state solutions with respect to the secondary emission coefficient, steady-state charging solutions for OSR coverglass were obtained for secondary emission coefficients ranging from .5 to .95. The results for eclipse and at winter-solstice, 8:00LT are shown in figure 6 along with the absolute potential of the spacecraft structure for the winter-solstice orbital period at 8:00 LT. It can be seen in figure 6 that for eclipse as the secondary emission coefficient increases the coverglass becomes increasingly more positive with respect to the S/C structure. This is to be expected since as the secondary coefficient increases there is more net positive current flow (less negative current flow) into the dielectric materials than into the metallic structure which has an assumed secondary emission coefficient of .5. Whereas, during winter-solstice at 8:00 LT as the coefficient decreases, the coverglass, which is self-shadowed, becomes increasingly negative with respect to the structure. As the coefficient decreases there is less net positive current flow (more negative current flow) to the OSR coverglass. The structural potential also becomes more negative as the secondary coefficient decreases; however, it is strongly affected by the photoemission currents both directly and indirectly.

ESCAP Code Improvements

Recent improvements have been incorporated in the ESCAP code to decrease the comuter time needed to execute a steady-state solution. From equations (7) and (8) the steady-state equations can be written as

$$\left[I_i - \frac{V_i - V_o}{R_i (V_i - V_o)} \right] = 0 \qquad (10)$$

for $1 \leq i \leq n$, and

$$\sum_{i=0}^{m} I_i = 0 \qquad (11)$$

The solution to this system of equations can be viewed as an optimization problem where equation (11), which represents a current balance condition, must be minimized while simultaneously satisfying the set of n nonlinear equations (10) which can be considered as constraint equations on the current balance condition. If the structural potential, V_o, is considered as an independent variable and the n surface potentials as dependent variables, then for a given value of V_s (structural absolute potential), a of each of the n variables V_i, for $1 \leq i \leq n$, can be found from (10) and the validity of the current balance value can be determined from (11). Since all of the terms of the left side of (10) are well-behaved, monotonic functions, a unimodal single variable sequential search technique (ref. 4) can be used to solve (10) for V_i when given a value of V_o, i.e., that value of V_i which minimizes (10) for a given value of V_o is the desired solution. Since (11) as a function of V_o represents the sum of monotonically decreasing or increasing functions, it also will be a unimodal function of V_o. Consequently, a single variable search technique can also be used to find that value of V_o which minimizes (11). This value of V_o represents the desired solution.

The Fibonacci sequential single variable search technique (ref. 4) was employed to minimize (solve) equations (10) and (11). The total range of possible surface potential values was divided into two regions and the search was conducted in one of these two possible regions for each surface. For surfaces with a positive or low negative potential, the range of potential values from +10V to -200V was iteratively searched. Within only twenty-two iterations the interval of uncertainty was reduced to .007 (a factor of 3×10^{-5}). For surfaces with a high negative potential the range of potential values from -200V to -40,000V was iteratively searched. Within only twenty iterations the interval of uncertainty was reduced to 3.5V (a factor of 10^{-4}). In the process of solving equations (10) and (11) by this approach it was found that the final net current incident to the total outside surface was a factor of 10^5 less than the initial net current flow to the spacecraft. It should also be noted that the search process produced the same solution after starting the search at a number of different initial starting points; this confirmed the unimodality assumption. In addition, the code has been programmed such that it can automatically determine which of the two regions should be searched for a particular surface, and the polarity of that surface.

Recently it has been proposed in reference 2 that the actual plasma particle current densities and energies could be adequately represented by a sum of two or more Maxwellian distributions. As can be seen from the S/C charging equations given previously, the form of the equations can readily accommodate two or more Maxwellian distributions and associated parameters. In addition, field-aligned fluxes can be included by simply altering the current sources to the particular surfaces of the S/C that are affected by the field aligned flux. The modified spacecraft charging equations would then have the form

$$
\begin{aligned}
\frac{V_1 - V_o}{R_1(V_1-V_o)} &= \sum_j I_{1j} \\
&\vdots \qquad\qquad \vdots \\
\frac{V_i-V_o}{R_i(V_i-V_o)} &= \sum_j I_{ij} + I_{f_i} \\
&\vdots \qquad\qquad \vdots \\
\frac{V_k-V_o}{R_k(V_k-V_o)} &= \sum_j I_{kj} + I_{f_k} \\
&\vdots \qquad\qquad \vdots \\
\frac{V_n-V_o}{R_n(V_n-V_o)} &= \sum_j I_{nj}
\end{aligned}
\tag{12}
$$

where the plasma generated net current flow to a surface is represented by a sum of j Maxwellian distributions and the i^{th} through k^{th} surfaces are affected by field aligned fluxes represented by an I_f equivalent current source. The above modifications to the spacecraft charging equations represent possible future improvements in the ESCAP code.

CONCLUSIONS

This paper has presented steady-state spacecraft charging results for the DSCS-III satellite during the equinox and winter-solstice orbital periods for a severe geomagnetic substorm. It was shown that only one of the outer dielectric surface materials, the OSR coverglass, could be a possible source of ESD in the steady-state. Conductive coatings have been used to control ESD on the dielectric structural parts of antennas operating at low frequencies. Silica cloth materials and blankets have been used to control ESD on most of the surfaces of the spacecraft. It was found that the steady-state solutions were strongly dependent on the value of the secondary electron emission coefficient.

At present, the computer model uses a single Maxwellian approximation to the actual plasma distribution and the substorm is assumed to be time-independent for the duration of the substorm. However, the spacecraft charging equations can easily accommodate a "two Maxwellian" approximation to the actual plasma distribution as well as field-aligned particle fluxes. Once the geometrical, electrical, and material configurations of a spacecraft have been defined and entered into the code, the steady-state solutions can be obtained at every hour over the orbital period from 23:00 LT to 8:00 LT with a small amount of computer execution time (typically 3-5 minutes).

REFERENCES

1. Massaro, M. J., Green, T., and Ling, D., "A Charging Model for Three-Axis Stabilized Spacecraft", Proc. of the S/C Charging Technology Conference, Feb., 1977, AFGL-TR-77-0051, NASA TMX-73537.

2. Garrett, H.B., "Modeling of the Geosynchronous Orbit Plasma Model - Part I," Dec., 1977, AFGL-TR-77-0288, Air Force Surveys in Geophysics, No. 380.

3. Condon, G. P., "Design Development of S/C Shielding Protection Against EMI from S/C Charging/Discharging Products", GE TIS No. 76SDS053, Dec., 1976.

4. Wilde, D. J., "Optimum Seeking Methods: Prentice-Hall, N.J., 1964.

Table 1. DSCS-III Material Parameter Summary

Surface	Material	Relative Dielectric Constant	Bulk Resistivity (Ω - cm)	Thickness (cm)	Capacitance (pf/cm^2)	Resistance ($\Omega-cm^2$)
1. Back-side	No. 527 silica cloth blanket	1.7	10^{15}	.030	5.0	3×10^{13}
2. West Panel	No. 527 silica cloth blanket	1.7	10^{15}	.030	5.0	3×10^{13}
3A. North Panel	No. 527 silica cloth blanket	1.7	10^{15}	.030	5.0	3×10^{13}
3B. N.P. Window	OSR glass	4.5	7.6×10^{15}*	.020	20.0	1.5×10^{14}
4A. South Panel	No. 527 silica cloth	1.7	10^{15}	.030	5.0	3×10^{13}
4B. S.P. Window	OSR glass	4.5	7.6×10^{15}*	020	20.0	1.5×10^{14}
5. East Panel	No. 527 silica cloth blanket	1.7	10^{15}	.030	5.0	3×10^{13}
6. Earth Side						
6A. MBA-RX 6B. MBA-TX1, TX2	No. 570/550/581 silica cloth composite	1.12	10^{16}	0.605	0.20	6.05×10^{15}
6C. GDA-TX 6D. E.C. - TX1, TX2 6E. E.C - RX1, RX2	No. 570 silica cloth	1.9	10^{16}	0.068	2.5	6.8×10^{14}
6F. S.P. Edge 6G. N.P. Edge	No. 527 silica cloth blanket	1.7	10^{15}	.030	5.0	3×10^{13}
6H. SCT-RX	Fiberglass with conductive ITO Coating	2.4		0.152	1.4	500KΩ+
6I. SCT-TX	Fiberglass with conductive ITO Coating	2.4		0.305	0.70	500KΩ+
7A. Solar Array - sunside	Solar array coverglass	7.0	4.8×10^{16}	.0152	40.8	7.3×10^{14}
7B. Solar Array - darkside	Chemglaze	2.1	3.3×10^{15}	0.005	37.2	1.65×10^{13}
7C. Solar Array Yoke - sunside	No. 527 silica cloth blanket	1.7	10^{15}	.030	5.0	3×10^{13}
7D. Solar Array Yoke - sunside	Chemglaze	2.1	3.3×10^{15}	0.005	37.2	1.65×10^{13}
7E. S.A. Yoke Window - Darkside	No. 527 silica cloth	1.7	10^{15}	.030	5.0	3×10^{13}
7F. Solar Array Yoke - Darkside	Chemglaze	2.1	3.3×10^{15}	0.005	37.2	1.65×10^{13}

* Includes both bulk and surface resistivities

+ Total surface resistance

Table 2. Surface Area Summary

SURFACE IDENTIFICATION	MATERIAL	AREA (CM^2)
1. BACKSIDE	#627 SILICA BLK.	52,075
	EXPOSED METAL	709
2. WEST PANEL	#627 SILICA BLK.	33,264
	EXPOSED METAL	842
3. NORTH PANEL	#627 SILICA BLK.	26,411
	OSR GLASS	19,286
	EXPOSED METAL	2,486
4. SOUTH PANEL	#627 SILICA BLK.	48,174
	OSR GLASS	7,200
	EXPOSED METAL	2,713
5. EAST PANEL	#627 SILICA BLK.	33,337
	EXPOSED METAL	1 118
6. EARTH SIDE	#627 SILICA BLK.	18,766
	#570 SILICA CLOTH	6 453
	#570/550/581 CLOTH COMPOSITE	23,596
	FIBERGLASS WITH ITO	37
	EXPOSED METAL	3,958
7. & 9. SOLAR ARRAY SUN SIDE	SOLAR ARRAY COMPOSITE	116,968
	#627 SILICA CLOTH (YOKE)	4,843
8. & 10. SOLAR ARRAY DARK-SIDE	CHEMGLAZE (INCLUDING YOKE)	122,649
11. PERMANENTLY SHADOWED AREAS	#627 SILICA BLK.	8,660
	FIBERGLASS WITH ITO	289
	EXPOSED METAL	10,681

Table 3. Photoemission, Secondary Emission and Omnidirectional Plasma Parameters

PARAMETER	TYPICAL RANGE	VALUE SELECTED
T_{ph}	$1\ V \leq T_{ph} \leq 3V$	2 V
T_e	$2\ V \leq T_e \leq 4\ V$	2 V
f_{om}	$0 \leq f_{om} \leq 1$	0.6
f_{od}	$0 \leq f_{od} \leq 1$	0.75
f_{pm}	$0 \leq f_{pm} \leq 1$	0.6
f_{pd}	$0 \leq f_{pd} \leq 1$	0.75
T_o	$1KV \leq T_o^* \leq 7.0KV$	2.3KV (MILD SUBSTORM) 5.3KV (MODERATE SUBSTORM) 7.0KV (SEVERE SUBSTORM)
T_p	$2.5KV \leq T_p^* \leq 10.4KV$	3.0 KV (MILD SUBSTORM) 5.8 KV (MODERATE SUBSTORM) 8.8 KV (SEVERE SUBSTORM)
J_{ph_o}	$0.82\ na/cm^2 \leq J_{ph_o} \leq 4\ na/cm^2$	$3\ na/cm^2$ (METALS) $0.9\ na/cm^2$ (DIELECTRICS)
J_{e_o}	$0.004na/cm^2 \leq J_{e_o}^* \leq 0.8\ na/cm^2$	$1.0na/cm^2$ (MILD SUBSTORM) $0.5na/cm^2$ (MODERATE SUBSTORM) $0.5na/cm^2$ (SEVERE SUBSTORM)
J_{p_o}	$2pa/cm^2 \leq J_{p_o}^* \leq 28\ pa/cm^2$	$18.5pa/cm^2$ (MILD SUBSTORM) $10pa/cm^2$ (MODERATE SUBSTORM) $10pa/cm^2$ (SEVERE SUBSTORM)

* THESE PARAMETERS REPRESENT A SINGLE MAXWELLIAN DISTRIBUTION APPROXIMATION TO THE ACTUAL MEASURED PARTICLE DENSITY AND ENERGY DISTRIBUTIONS. PARAMETER VALUES WERE SUPPLIED BY THE AIR FORCE GEOPHYSICAL LABORATORY, HANSCOM AFB, MASS.

Table 4. Summary of Steady-State Results For A Severe Substorm During Fall-Equinox

LOCAL TIME	MATERIAL WITH THE MAXIMUM POTENTIAL DIFFERENCE OSR GLASS ON NORTH AND SOUTH PANELS	ABSOLUTE POTENTIAL OF S/C STRUCTURE (VOLTS)
23:00	- 5160	- 240
24:00 (ECLIPSE)	160	- 14160
1:00	- 5160	- 235
2:00	- 5165	- 210
3:00	- 5165	- 205
4:00	- 5165	- 210
5:00	- 5165	- 220
6:00	- 4780	- 1490
7:00	- 5165	- 220
8:00	- 5170	- 200

Table 5. Summary of Steady-State Results for a Severe Substorm During Winter-Solstice

LOCAL TIME	MATERIAL WITH THE MAXIMUM POTENTIAL DIFFERENCE (VOLTS)	ABSOLUTE POTENTIAL OF S/C STRUCTURE (VOLTS)
	OSR GLASS ON NORTH PANEL	
23.00	- 5175	- 175
24:00	- 5170	- 190
1:00	- 5175	- 175
2:00	- 5200	- 170
3:00	- 5175	- 175
4:00	- 5170	- 180
5:00	- 5170	- 180
6:00	- 5170	- 200
7:00	- 5170	- 180
8:00	- 5175	- 175

Table 6. Summary of Maximum Potential Differences of Outer Surfaces During a Severe Geomagnetic Substorm

		MAXIMUM POTENTIAL DIFFERENCE BETWEEN SURFACE AND S/C STRUCTURE (VOLTS)
1.	BACK-SIDE NO. 527 SILICA CLOTH BLANKET	-220
2.	WEST PANEL, NO. 527 SILICA CLOTH BLANKET	±170
3.	NORTH PANEL, NO. 527 SILICA CLOTH BLANKET	-170
4.	NORTH PANEL, OSR GLASS COMPOSITE	-5200
5.	SOUTH PANEL NO. 527 SILICA CLOTH BLANKET	190
6.	SOUTH PANEL, OSR GLASS COMPOSITE	-5200
7.	EAST PANEL, NO. 527 SILICA CLOTH BLANKET	230
8.	EARTH SIDE, NO. 527 SILICA CLOTH BLANKET	225
9.	EARTH SIDE, NO. 570 SILICA CLOTH	240
10.	EARTH-SIDE, NO. 570/550/581 SILICA CLOTH COMPOSITE	-200
11.	EARTH-SIDE, CONDUCTIVELY COATED FIBERGLASS	-2
12.	SOLAR ARRAY, SOLAR ARRAY COVER GLASS	1500
13.	SOLAR ARRAY, CHEMGLAZE PAINT	-1370
14.	PERMANENTLY SHADOWED, CONDUCTIVELY COATED FIBERGLASS	-2
15.	PERMANENTLY SHADOWED, NO. 527 SILICA CLOTH	-160

Table 7. ESD Probabilities of Occurrence For the OSR Glass Composite Material During A Severe Substorm*

NO. OF ESD DISCHARGES OCCURRING AT RANDOM TIMES IN ONE SECOND	PROBABILITY OF OCCURRENCE
≥ 1	0.642
≥ 2	0.264
≥ 3	0.0755
≥ 4	0.016
≥ 5	2.6×10^{-3}
≥ 6	3.3×10^{-4}
≥ 7	3.4×10^{-5}
≥ 8	3×10^{-6}
≥ 9	2×10^{-7}
≥ 10	1×10^{-8}

* THE SEVERE SUBSTORM WAS SIMULATED BY BOMBARDING THE OSR GLASS MATERIAL SAMPLE WITH 20 KeV ELECTRONS HAVING A CURRENT DENSITY OF 1.5 NA/CM^2

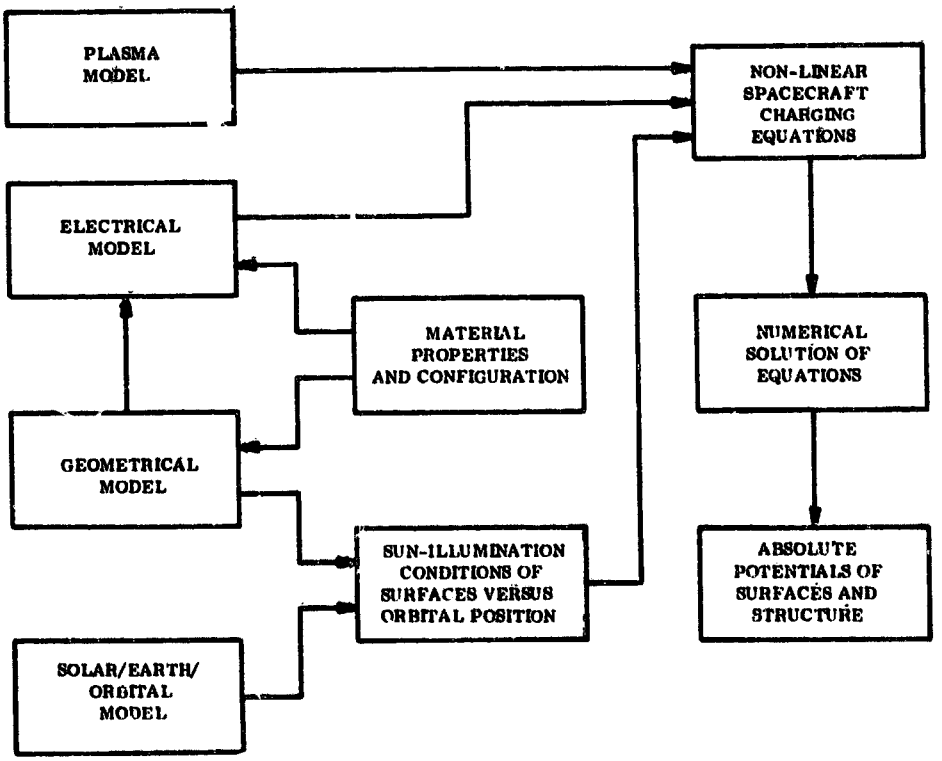

Figure 1. Spacecraft Charging Model Flow Chart.

C-3

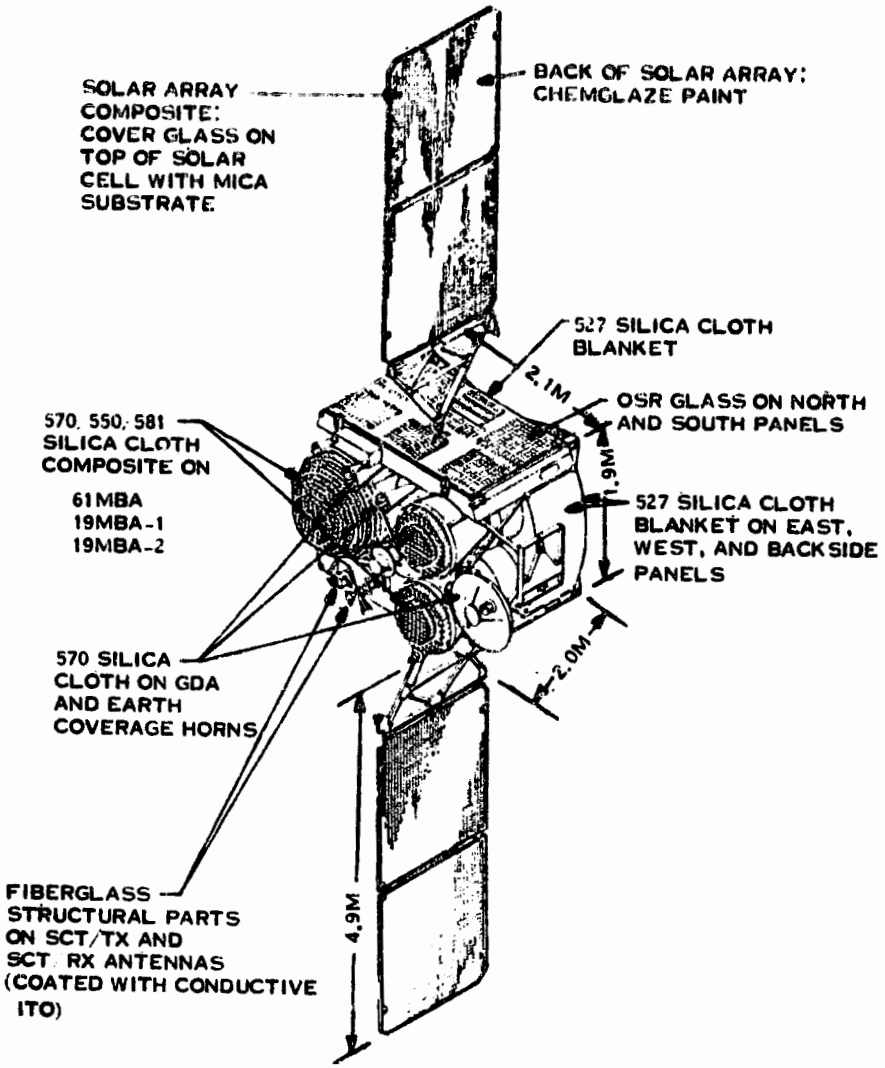

Figure 2. DSCS-III Material Configuration.

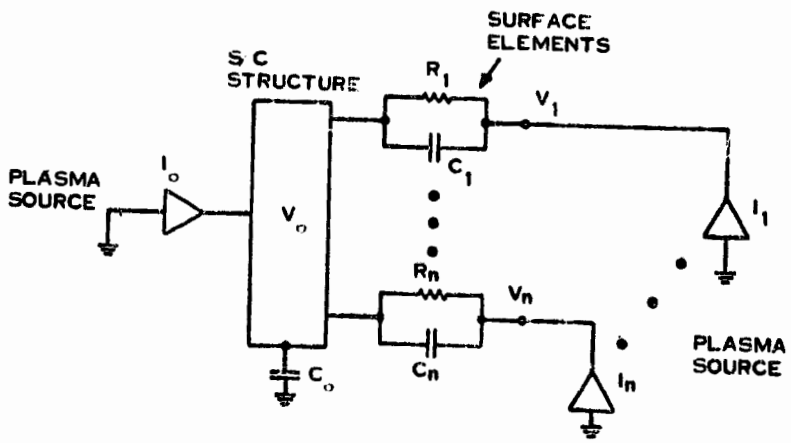

Figure 3. Spacecraft Equivalent Circuit

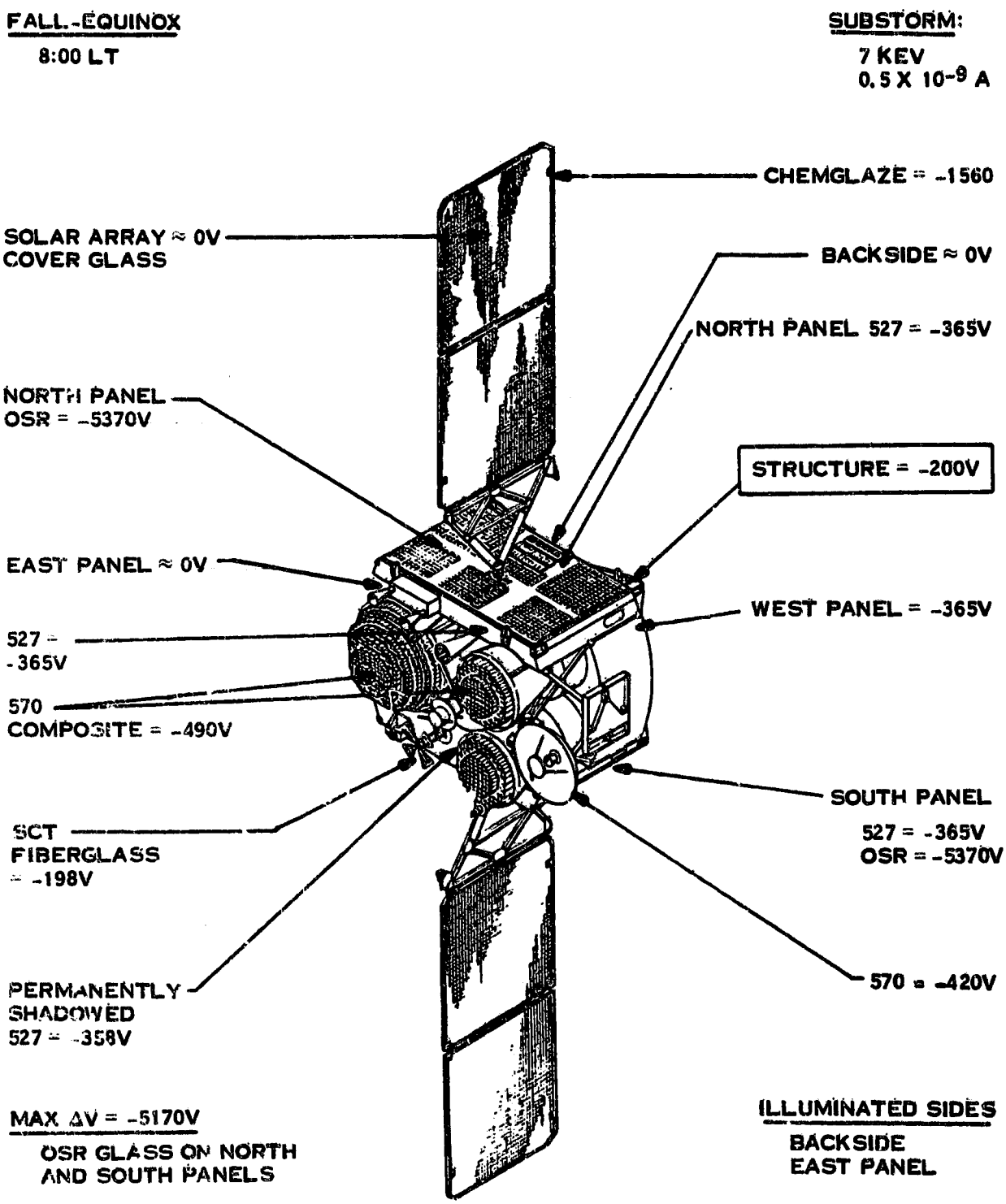

Figure 4. Steady-State Absolute Potentials of DSCS-III at 8:00 L.T. (Fall-Equinox) For A Severe Substorm

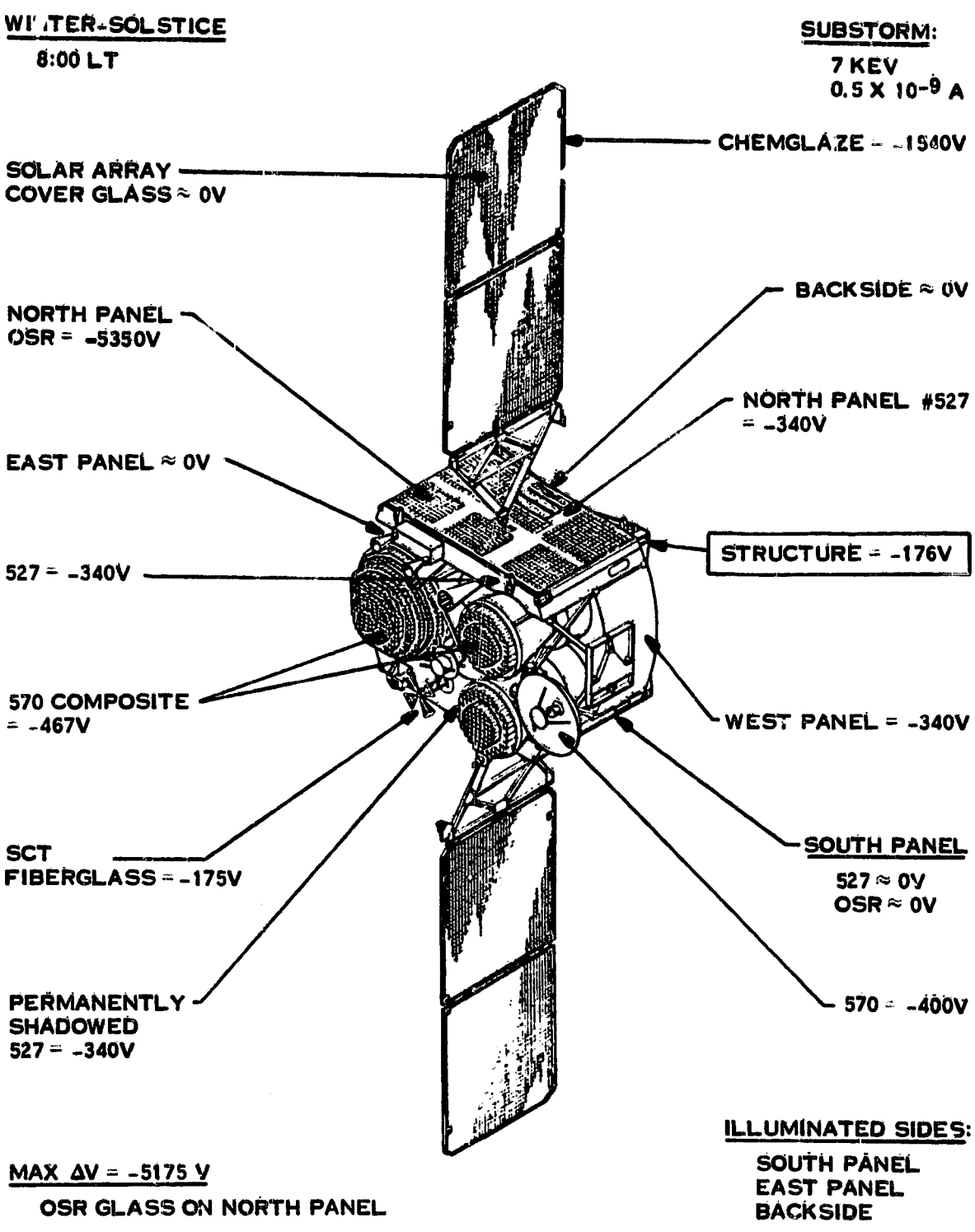

Figure 5. Steady-State Absolute Potentials of DSCS-III at 8:00 L.T. (Winter-Solstice) During A Severe Substorm.

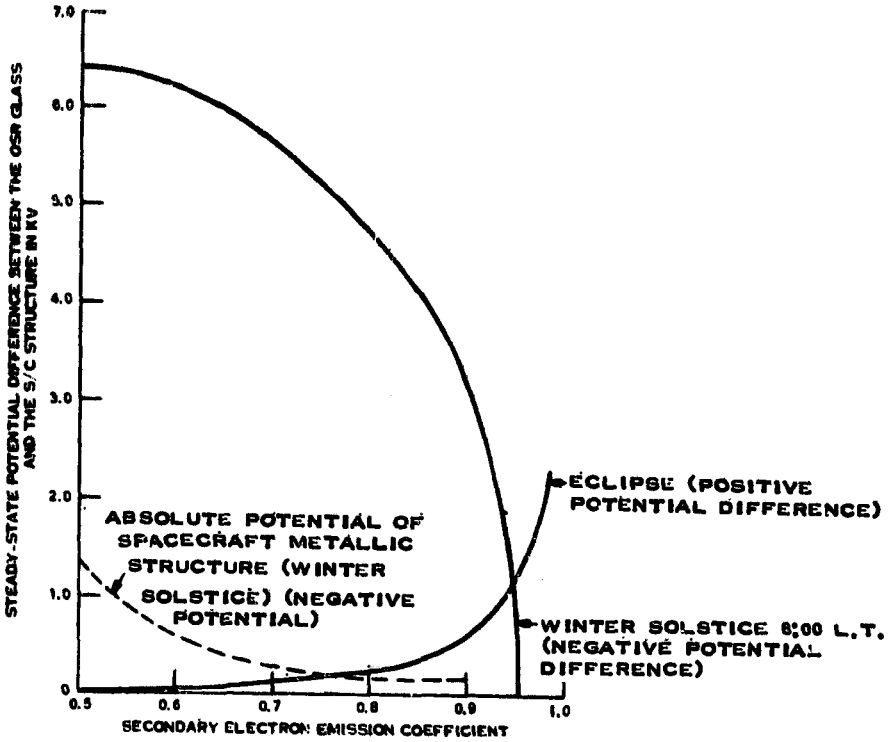

Figure 6. Variation of Steady-State Differential Potential As A Function of Secondary Electron Emission Coefficient